International Journal of Networks and Communications 2018, 8(3): 63-80
DOI: 10.5923/j.ijnc.20180803.02

Effect of Four-Wave Mixing on the Transmission Performance of O-Band Multichannel PAM-Based Unamplified Datacenter Interconnects

Duha S. Ahmed*, Raad S. Fyath

Department of Computer Engineering, Al-Nahrain University, Baghdad, Iraq

Abstract Optical links incorporating multilevel pulse amplitude modulation (PAM) with intensity modulation/direct detection (IM/DD) scheme have shown promising features when used as low-cost data center interconnects. This paper addresses the transmission performance of PAM-based wavelength division multiplexing (WDM) interconnect operating in the O-band with 112 Gbps channel data rate and 200 GHz channel spacing and without using optical amplification. The effect of four-wave mixing (FWM), associated with nonlinear fiber optics, on the transmission performance of the unamplified O-band PAM-WDM interconnect is investigated analytically. Simulation results, obtained using Optisystem ver. 15, are then presented for eight different Scenarios, namely 4-PAM 4WDM, 8-PAM 4WDM, 4-PAM 8WDM and 8-PAM 8WDM operating in the absence and presence of polarization interleaving (PI). The results reveal that using PI enhances the transmission performance of O-band PAM-WDM interconnects and this effect is more pronounced for 4-PAM system. At 0 dBm channel launch power, the maximum reach for the 4-PAM 8-WDM interconnect increases from 10 to 42 km by applying PI. These values are to be compared with 38 to 44 km, 8 to 36, and 2 to 10 km, for 4-PAM 4-WDM, 8-PAM 4-WDM, and 8-PAM 8-WDM, respectively.

Keywords Intensity modulation/direct detection (IM/DD), Data center optical interconnects, Optical pulse amplitude modulation (PAM), Wavelength-division multiplexing (WDM), Four-wave mixing (FWM), Polarization interleaving (PI)

1. Introduction

Recently, there is exponential increase in traffic demand in optical networks to cover bandwidth hungry applications such social networking, cloud computing, and high definition TV and video [1-4]. This increasing demand has triggered different research groups to investigate the performance of high-speed datacenter interconnects implemented using high-order modulation formats and advanced multiplexing techniques [5-8]. The current 10 and 40 Gbps wavelength-division multiplexing (WDM) solutions employed in short-reach optical networks are not able successfully to keep up with the ever-growing demand [7]. Recent standardization works have been focused on delivering 100 and 400 Gbps alternatives for short-reach applications [9, 10]. Since cost and robustness are major concerns, intensity modulation/direct detection (IM/DD) technique (i.e., noncoherent technique) is strongly recommended for implementing these advanced interconnects over coherent techniques [11-14]. The main features of IM/DD technique are

(i) Intensity modulation can be implemented efficiently using directly modulated laser (DML) [15-18] or externally modulated laser (EML) [13-19] without the need of in-phase quadrature-phases (IQ) optical modulator.

(ii) Direct detection has advantages of low cost and easy integration compared with coherent detection. The DD needs one single-end photodiode (PD) and one analog-to-digital converter (ADC) [20, 21]. In contrast, coherent receiver requires complex hardware including local laser, to act as a local oscillator and should be synchronized with the transmitter laser, balanced PDs, and more than one ADC [22].

Optical data center interconnects (DCIs) based on multilevel pulse modulation (M-PAM) technique have attracted increasing interest for short-reach applications [23, 24]. The main motivations behind this interest are

(i) The optical M-PAM interconnect can be efficiently implemented using IM/DD communication system and hence gains the main advantages and merit

* Corresponding author:
duhasabah94@gmail.com (Duha S. Ahmed)
Published online at http://journal.sapub.org/ijnc

behind this system.

(ii) The PAM modulation is obtained using robust and low-cost modulator configurations based on either DML [25] or EML [26, 27]. The second configuration is also applicable for dual-polarization multiplexing (DPM) and can be used to double the transmission data rate compared with single-polarization (SP) counterpart.

(iii) The PAM is less complex than other advanced modulation techniques used for short-reach applications such as orthogonal frequency-division multiplexing (OFDM) [28] and carrierless amplitude/phase (CAP) modulation [29] which can be implemented using IM/DD configuration. The OFDM and CAP modulation are more complex than PAM since OFDM uses fast Fourier transform (FFT) and inverse FFT while the CAP uses orthogonal filter pairs at the transmitter and receiver [30].

Recently, there is increasing interest in PAM-based optical interconnects capable of carrying 100 Gbps and beyond data rates. These interconnects should match the requirements handled by 100 Gigabit Ethernet (GbE), 400 GbE, and 1 Terabit Ethernet (TbE) standards. Mardoyan et al. [31] demonstrated the transmission of 150 Gbps 8-PAM signal over 2 km of standard single-mode link (SSMF) and 100 Gbps 4-PAM signal over 4 km of SSMF. The link operates at 1550 nm wavelength without optical amplification. Working at longer distance at this wavelength requires careful equalization for the fiber chromatic dispersion (CD) which is around 17 ps/(nm.km) [32]. This encourages researches to use 1310 nm window, where CD is almost negligible, for transmission the data over the PAM-based interconnects. El-Fiky [23] demonstrated 168 Gbps single-carrier 4-PAM transmission over 10 km SSMF using O-band laser operating at 1325 nm. A 224 Gbps PDM 4-PAM transmission over 10 km SSMF was demonstrated at 1310 nm by Morsy-Osman without using optical amplifier [11].

Wavelength-division multiplexing technique has been also applied to enhance the capacity of the PAM interconnected beyond 100 Gbps. For example, Eiselt [6] demonstrated 8×56.25 Gbps (400 Gbps) 4-PAM DCI operating over 80 km of SSMF at C-band. The link was supported by optical amplification and dispersion compensation fiber (DCF). The main challenge behind the use of WDM to enhance the capacity of PAM interconnect is fiber nonlinear optics. The dependence of fiber refractive index and optical intensity according to Kerr effect gives rises to different nonlinear process such as four-wave mixing (FWM). The effects of FWM on the performance of C-band WDM system, designed with 50 GHz (or more) channel spacing, is small due to the relative high fiber CD in this band which introduces phase mismatch between the four waveforms involved in this process. In contrast, FWM may degraded the performance of the O-band WDM where CD is almost negligible in this band.

The aim of this paper is to address the possibility of using 4×112 Gbps and 8×112Gpbs WDM systems to enhance the capacity of unamplified 4- and 8-PAM O-band datacenter interconnects. The effect of fiber nonlinear optics on the transmission performance is addressed analytically and supported by simulation based on a Optisystem software ver. 15.

2. Investigation of FWM in O-Band WDM Interconnects

2.1. Background

Four-wave mixing is a nonlinear fiber process which occurs due to the dependence of fiber refractive index n on the intensity of the propagation waves according to Kerr effect [33]

$$n = n_0 + n_2 I \quad (1)$$

where n_0 is the linear fiber refractive index and n_2 is the nonlinear refractive index coefficient. In this phenomenon, the energy of two photons of frequency f_i and f_j are converted into two new photons of frequencies f_k and f_m. The energy of a photon of frequency f is given by hf where h = 6.6026×10^{-34} Js is Planck's constant. Therefore, applying energy conservation law to the FWM process reveals that

$$f_k + f_m = f_i + f_j \quad (2a)$$

when i=j, two photons of frequency fi enter the FWM process to produce two new photons of frequencies f_k and f_m such that $f_m+f_k = 2f_i$. In this case, the process is called degenerate FWM (DFWM). Figure 1 illustrates the concepts of both nondegenerate FWM (NDFWM) and DFWM processes.

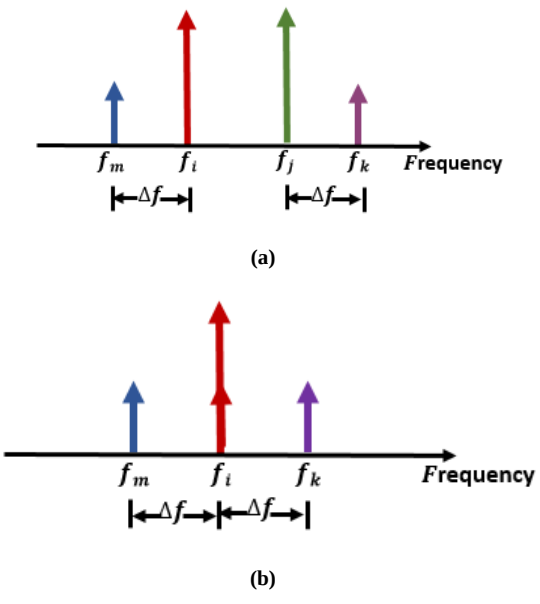

Figure 1. Concepts of four-wave mixing (FWM) in the frequency domain (a) nondegenerate four-wave mixing (NDFWM) (b) degenerate four-wave mixing (DFWM)

FWM may play a key role in degrading the performance of WDM system since it generates new frequencies that may coincident with other channels frequencies. In this case, the FWM process can be described as the interaction of three optical waveforms of frequencies f_i, f_j, and f_k via nonlinear fiber optics to generate new waveform of frequency $f_{ijk} \equiv f_m$

$$f_{ijk} \equiv f_m = f_i + f_j - f_k \quad (2b)$$

where i, j and k vary from 1 to N (N is the number of WDM channels). This results in large number of FWM components [34]

$$N_{FWM} = N^2(N-1)/2 \quad (3)$$

For N = 4, 8, and 16 WDM systems, N_{FWM}= 24, 224, and 1920.

The power transferred to the FWM component at the fiber end is given by [34]

$$P_m(L) = \eta_{FWM} (\gamma L)^2 P_i P_j P_k e^{-\alpha L} \quad (4)$$

where L is the fiber length, η_{FWM} is the efficiency of the FWM process, γ is the nonlinear fiber parameter ($\gamma=2\pi n_2/\lambda A_{eff}$) with λ is the operating wavelength and A_{eff} is the effective fiber core area. Further, P_x (x=i, j, and k) represents the xth-channel launched power at the fiber input and α is the fiber loss coefficient measured in km^{-1}. The FWM efficiency is defined as [34]

$$\eta_{FWM} = \alpha^2 /(1-e^{-\alpha L})^2 \left| 1-\exp[-(\alpha+j\Delta k)L]/(\alpha+j\Delta k) \right|^2 \quad (5)$$

where Δk is the phase mismatch which will be explained later in this subsection. Using Euler identity $\exp(-j\Delta kL) = \cos(\Delta kL) - j\sin(\Delta kL)$ into eqn. 5 yields

$$\eta_{FWM} = \alpha^2/(1-e^{-\alpha L})^2[1-e^{-\alpha L}\cos(\Delta kL)]^2 + e^{-2\alpha L}[\sin(\Delta kL)]^2/[\alpha^2+(\Delta k)^2]$$

$$= \alpha^2/(1-e^{-\alpha L})^2 (1-2e^{-\alpha L}\cos(\Delta kL) + e^{-2\alpha L} / [\alpha^2+(\Delta k)^2]) \quad (6)$$

For the special case of negligible fiber loss (i.e., $\alpha L \ll 1$), eqn. 6 reduces to

$$(\eta_{FWM})_{\alpha=0} = 2[1- \cos(\Delta kL)]/ (\Delta kL)^2 = 0.5\, \mathrm{sinc}^2(\Delta kL/2) \quad (7)$$

where $\mathrm{sinc}(\theta) \equiv \mathrm{sinc}(\theta)/\theta$ is the sinc function. Note that $(\eta_{FWM})_{\alpha=0.5}$ when $\Delta kL \ll 1$.

In the presence of fiber loss and perfect phase matching condition (Δk=0), then eqn. 6 tends to $(\eta_{FWM})_{\Delta k=0}$ = 100%.

The phase mismatch Δk arises since the four waveforms involved in the FWM process don't propagate at the same speed through the fiber. The parameter Δk can be expressed as the sum of two parts Δk_L and Δk_{NL}. The linear part Δk_L comes from the dependence of fiber refractive index on the operating wavelength. Therefore, Δk_L is usually described by Δk_{mat} since it represents the contribution of fiber material dispersion. The nonlinear phase mismatch Δk_{NL} comes from the contribution of fiber nonlinear optics.

The parameter Δk_L is described by the following expression [33]

$$\Delta k_L = (2\pi\lambda_0^2/2)(f_i-f_k)(f_j-f_k)[D(\lambda_0) - \lambda_0^2((f_i+f_j)/2)-f_m S(\lambda_0)] \quad (8)$$

where λ_o is the reference wavelength. Note that Δk_L depends on the dispersion parameters (GVD and dispersion slope) and it is independent of fiber nonlinear refractive index coefficient n_2.

The nonlinear phase mismatch component Δk_{NL} is expressed as [35]

$$\Delta k_{NL} = \gamma (P_i + P_j - P_k)(1-e^{-\alpha L}/\alpha L) \quad (9)$$

where P_i, P_j, and P_k are the powers of the three input FWM waveforms estimated at the fiber input.

Consider an N-channel WDM systems operating with equal channel spacing Δf and equal optical launch power P_0, ($P_i = P_0$ for i=1, 2, ..., N). Then eqn. 4 reads as follows to describe the power of the FWM components at the fiber link

$$P_m(L) = \eta_{FWM} (\gamma L)^2 P_0^3 e^{-\alpha L} \quad (10)$$

For the DFWM, the frequency of two photons entering the FWM process is $f_i=f_j$ (see Figure 1b), then the equal channel spacing condition yields

$$f_i-f_k = f_j-f_m = -\Delta f \quad (11)$$

According to eqn. 8, the linear part of the phases mismatch Δk_L becomes

$$\Delta k_L = (2\pi/c) \lambda_0^2 (\Delta f)^2 D(\lambda_0) - (2\pi\lambda_0^4/c^2) (\Delta f)^3 S(\lambda_0) \quad (12)$$

At 1550 nm window, the effect of the dispersion parameter D dominates and hence the effect of dispersion slope can be neglected. The eqn. 12 reduces to

$$\Delta k_L|_{1550\ nm} = (2\pi/c) \lambda_0^2 (\Delta f)^2 D(\lambda_0) \quad (13a)$$

At zero-dispersion wavelength (≈1310 nm for SSMF), the dispersion slope S plays a key role in determining the linear phase mismatch in that band

$$\Delta k_L|_{1310\ nm} = -(2\pi/c^2) \lambda_0^4 (\Delta f)^3 S(\lambda_0) \quad (13b)$$

Note that λ_0 = 1550 nm and 1310 nm should be used in eqns. 13a and 13b, respectively. Therefore,

$$r_{\Delta k} \equiv \frac{\Delta k_L|_{1310\ nm}}{\Delta k_L|_{1550\ nm}} = -\frac{1}{c}\frac{\lambda_1^4 S(\lambda_1)}{\lambda_2^2 D(\lambda_2)} \Delta f \quad (14)$$

where λ_1=1310 nm and λ_2=1550 nm. Let D = 17 ps/(nm.km) at 1550 nm and S = 0.092 ps/(nm^2.km) at 1310 nm, then $|r_{\Delta k}| = 2.2\times10^{-20}\ \Delta f$.

2.2. Effect of Interconnect Parameters on FWM Efficiency

This subsection presents results describing the effect of the dispersion parameters and length of the interconnect on the FWM efficiency. The calculations are performed for unamplified 4-PAM WDM link designed in the O-band with 200 GHz channel spacing to carry 112 Gbps per channel data rate. For comparison purposes, results related to C-band counterpart are also given.

Figure 2 shows the dependence of η_{FWM} on the interconnect length for the 1550 nm system and taking the dispersion parameter D as an independent parameter and assuming α_{dB}= 0.2 dB/km. The calculations are based on eqn. 13a and presented for three values of D, 1, 5, and 17 ps/(nm.km). The 17 ps/(nm.km) dispersion is related to a SSMF operating at 1550 nm window while 1 and 5 ps/(nm.km) dispersions are related to a SSMF designed with partially dispersion compensation scheme. Note that

for this value of channel spacing (200 GHz), the effect of FWM is almost negligible when D = 17 and 5 ps/(nm.km) for all values of transmission distance. The statement is also true for D = 1 ps/(nm.km) and L > 5 km.

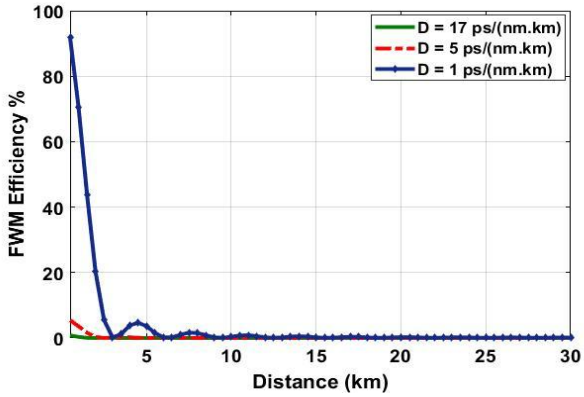

Figure 2. Variation of FWM efficiency with fiber transmission length for the 1550 system

The variation of η_{FWM} with the 1310 nm fiber link is illustrated in Fig. 3. The results are presented for three values of dispersion slope (0.05, 0.1, and 0.15 ps/(nm^2.km)) and obtained using eqn. 13b with α_{dB}= 0.35 dB/km. Note that the efficiency is a decreasing function of both dispersion slope and link length. At L= 7, 10, and 22 km, the efficiency equals 80% when S= 0.05, 0.1, and 0.15 ps/(nm^2.km), respectively. The 60% efficiency is obtained when L increases to 10, 15, and 37 km, respectively.

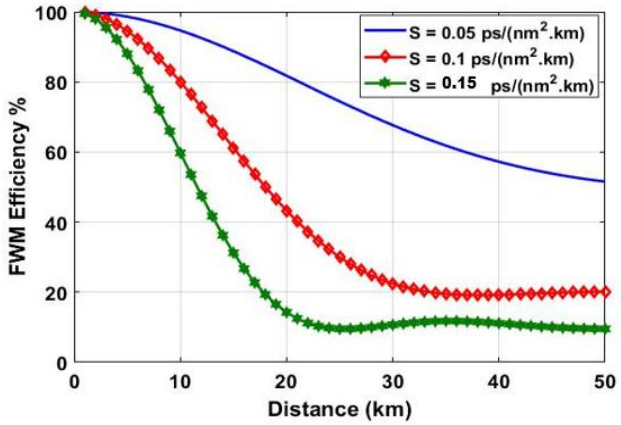

Figure 3. Variation of η_{FWM} with transmission distance for the 1310 nm system

The calculations are carried further to investigate the dependence of the power of the FWM component on various system parameters assuming O-band WDM system and using eqn. 10. The fiber parameters values at 1310 nm that used in the following calculations and simulations are α_{dB}=0.35 dB/km, S=0.092 ps/(nm^2.km), effective area A_{eff}=80 μ^2 m, and n_2 =26×10^{-21} m^2/W. The nonlinear fiber parameter $\gamma = 2\pi n_2/(\lambda_0 A_{eff})$=1.56 W^{-1} km^{-1} at λ_0 =1310 nm. Equation 10 can be expressed in logarithmic scale to see the variation of the FWM component power with single channel power P_0 using dBm measure

$$P_m(L)|_{dBm} = 10\log \eta_{FWM} + 20\log \gamma + 20\log L - 4.34\,\alpha L + 3P_0(dBm)$$

$$= 10\log \eta_{FWM} + 20\log \gamma + 20\log L - \alpha_{dB} L + 3P_0(dBm) \quad (15)$$

where $\alpha_{dB} = 4.34\alpha$ which denotes fiber loss in dB/km with α is measured in km^{-1}. Further, $P_m(L)|_{dBm} = 30+10\log[P_m(L)]$ and $P_0(dBm) = 30 + 10\log[P_0(W)]$ and indicate dBm measures for the two powers.

Investigating eqn. 15 reveals the following facts. The FWM component power $P_m(L)|_{dBm}$ increases linearly with channel launch power P_0 (dBm) with slope = 3. Increasing P_0 (dBm) from 0 to 3 dBm will increase the FWM component power by 9 dBm. This is to be compared with 30 dB increase in P_L (m) when P_0 (dBm) increases from 0 to 10 dBm.

It is clear the fiber length affects the level of P_m (L) on two opposite ways. Increasing the fiber length means increasing the length of the nonlinear fiber optics medium which leads to increase in the level of P_m (L). At the same time, increasing L means increasing the total fiber loss and decreasing the FWM efficiency which is also a function of both fiber length and loss coefficient. The two effects are balanced at certain link length L_0 which makes Pm attends its maximum value, $(P_m)_{max}$. The value of L_0 can be estimated by setting the derivative of the term $Q_{FWM} \equiv \eta_{FWM} (\gamma L)^2 e^{-\alpha L}$ with respect to L, to zero. If the variation of η_{FWM} with L is not taken into account, then dQ_{FWM}/dL attends to zero when $L_0=2/\alpha$ for α=0.08 km^{-1}, (i.e., α_{dB}= 0.35 dB/km) L = 25 km. The actual value of L_0 is less than that since η_{FWM} generally deceases with distance.

The dependence of FWM component power Pm on the fiber length is presented graphically in Fig. 4 for three values of channel launch power, P_0 = 0, 5, and 10 dBm. At 10 km, P_m = -40.4, -24.4, and -10.4 dBm when P_0 = 0, 5, and 10 dBm, respectively. Increases L beyond 10 km will increases Pm slightly till it approaches a maximum value at L ≡ L_0 = 16 km. when L>L_0, P_m decreases with L due to fiber loss. The effective fiber loss $(\alpha_{dB})_{eff}$ is about 0.22 dB/km when L varies from 20 to 100 km and this effective loss is independent of launch power P_0. The value of $(\alpha_{dB})_{eff}$ is estimated from

$$(\alpha_{dB})_{eff} = [P_m(20\text{ km})|_{dBm} - P_m(100\text{ km})|_{dBm}]/(100-20) \quad (16)$$

The linear effective loss $\alpha_{eff} = (\alpha_{dB})_{eff}/4.34$=0.0507 km^{-1}. Note that $(\alpha_{dB})_{eff}$ is lower than 0.35 dB/km which is the loss of SSMF operating in the absence of nonlinear fiber optics effects. Note further that the FWM process try to enhance the level of the FWM component with increasing L due to the increase of the length of the nonlinear fiber optics medium.

The analysis is carried further to deduce a simplified expression for the effective fiber loss parameter $(\alpha_{dB})_{eff}$ when the variation of η_{FWM} with distance is not taken into account. When the fiber operates in the linear region, the

signal power at a distance L is related to its power at a reference distance L_r by [36]

$$P(L) = P(L_r)\, e^{-\alpha(L-Lr)} \quad (17a)$$

Therefore, α is defined as

$$\alpha = -\frac{dP(L)}{dL} / P(L) \quad (17b)$$

Equations (17a) and (17b) are modified in this work to describe the loss of a fiber operating in the nonlinear region

$$P_m(L) = P_m(L_r)\, e^{-\alpha eff(L-Lr)} \quad (18a)$$

$$\alpha_{eff} = -\frac{dP_m(L)}{dL} / P_m(L) \quad (18b)$$

According to the results depicted in Fig. 4, L_r =20 km and eqns. 18a and 18b valid for L>20 km. Using eqn. 10, which describes the variation of FWM component power with distance, into eqn. 18b yields $\alpha_{eff} = \alpha - 2/L$. Note that α_{eff} is length dependent and yields $(\alpha_{eff})_{dB} = 4.43\alpha_{eff} = \alpha_{dB} - 8.68/L$ dB/km where α_{dB} is loss coefficient of the SSMF at the linear region (α_{dB}=0.35 dB/km at λ=1310 nm). This simplified predication gives α_{eff} = 0.051 km^{-1} [$(\alpha)_{dB})_{eff}$ = 0.22 dB/km)] at L = 66.8 km.

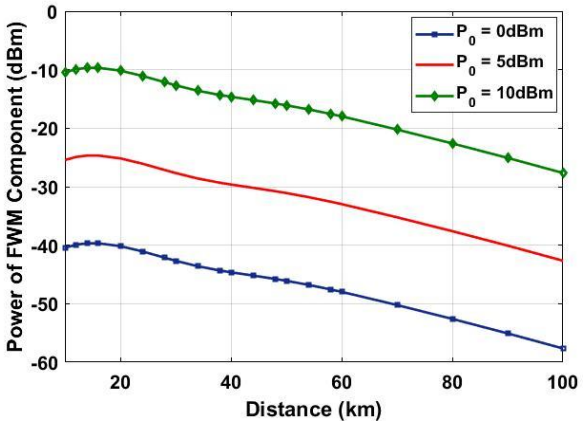

Figure 4. Variation of FWM component power P_m with the fiber length at 1310 nm

3. Design Issues for O-Band PAM WDM Interconnects

This section discusses design issues and presents initial simulation transmission results for WDM interconnects incorporating 4- and 8-PAM modulation formats. The interconnects are designed for O-band operation with 200 GHz channel spacing to support the transmission of 112 Gbps data rate per channel. The results are presented for 4- and 8-channel WDM systems and give feasibility study on design DCIs to support 400 GbE and 800 GbE. The operation of each of the WDM channel is based on IM/DD scheme implemented using DML-based optical transmitter and unamplified SSMF link. The following results and related discussion focus on the effect of FWM on the transmission performance.

As a starting point, which is useful for next discussion and comparison, the maximum transmission distance L_{max} corresponding to a single-channel link is deduced as a function of channel launch power. The values of L_{max} are estimated from the simulation when the receiver BER equals a threshold level (BER_{th}) of 4.4×10^{-3}. Recall that this BER limit represents the threshold of 7% overhead hard-decision (HD) forward error correction (FEC) code which yields 10^{-15} BER when the code is used. Figure 5 shows the dependence of L_{max} on launch power for a single-channel link and presented for both 4- and 8-PAM systems. Note that L_{max} increases almost linearly with launch power P_0(dBm) with slope ≈ 2.75 km/dBm for both PAM formats. At a fixed launch power, the value of L_{max} in the 4-PAM link exceeds that of the 8-PAM link by about 6-8 km. At P_0 = 10 dBm, the 4- and 8-PAM links are able to transmit the 112 Gbps data over 73 and 66 km, respectively.

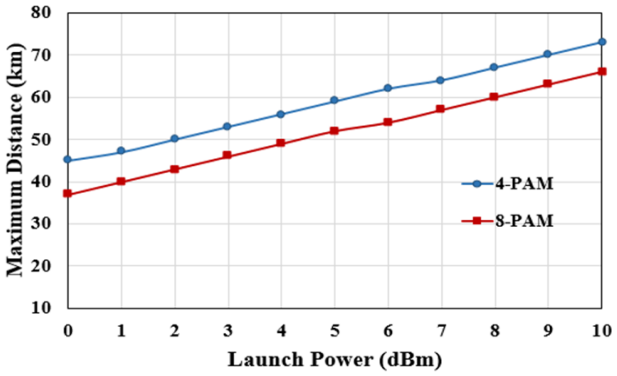

Figure 5. Variation of maximum transmission distance with launch power for 112 Gbps single-channel PAM link

3.1. WDM System Configuration

Figure 6 shows a simplified block diagram for a PAM-based 4-channel WDM link. The multiplexer (MUX) and the demulitplexer (DEMUX) act as 4:1 wavelength combiner and 1:4 wavelength-selective splitters, respectively. The demultiplexer is simulated here using four parallel optical bandpass filters (OBPFs) whose center frequencies match the frequencies of the four unmodulated transmitter lasers. The lasers frequencies are selected according to the O-band WDM grid issued by ITU-T (International Telecommunication Union-Telecommunicati on Standardization Sector) [37]. The grid fixes the lasers frequencies that should be used with 50 GHz channel spacing and these frequencies are distributed symmetrically around central frequency (taken here as 228.85 THz which corresponds to λ = c/f = 1310.00 nm, where c = 299.8×10^6 m/s is the speed of light in free space). The N-channel WDM system should be designed by selecting N frequencies from the grid with channel spacing n×50 GHz where n is a positive integer chosen to satisfy negligible crosstalk among the demultiplexer outputs.

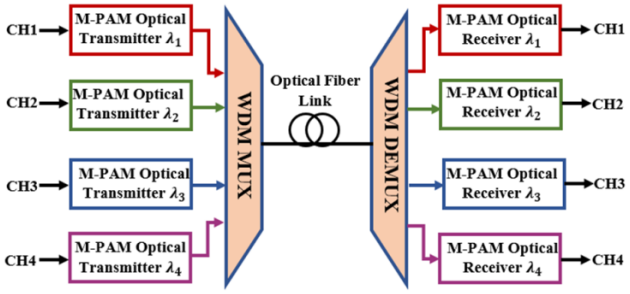

Figure 6. Block diagram for PAM-based 4-channel WDM link

Initial simulation test on the designed 4-PAM WDM link reveals that channel spacing Δf= 200 GHz (or more) should be used to prevent spectral overlapping between adjacent channels at the multiplexer output when 112 Gbps data is transmitted by each channel and this helps the demultiplexer to select the required channel with negligible crosstalk. Therefore, the lasers frequencies in this work are chosen according to the following formula

$$f_i\,(\text{THz}) = 228.85+[i-(0.5N+1)]\,(0.2)\;\; i=1,\,2,\,\cdots,\,N \qquad (19)$$

For the 4-channel WDM link, the frequencies of the transmitter lasers are tuned to f_1 = 228.45 THz, f_2 = 228.65 THz, f_3 = 228.85 THz, and f_4 = 229.05 THz. These frequencies correspond to the following wavelengths: λ_1= 1313.332 nm, λ_2= 1311.174 nm, λ_3= 1310.00 nm, and λ_4= 1308.884 nm. Note that the 200 GHz channel frequency spacing equals approximately 1.15 nm wavelength channel spacing. When 8-channel WDM link is used, the lasers frequencies are set to (in THz): to f_1 = 228.05, f_2 = 228.25, f_3 = 228.45, f_4 = 228.65, f_5 = 228.85, f_6 = 229.05, f_7 = 229.25, and f_8 = 229.45. The wavelength range spans from λ_1 = 1314.624 nm to λ_8 = 1306.63 nm.

3.2. Initial Simulation Tests

Many simulation tests are performed to assess the dependence maximum transmission distance L_{max} on channel launch power P_0 for the 4- and 8-channel WDM links operating with 4- and 8-PAM modulation formats. The results (which will be shown in Section 4) indicate that two distinct regions can be seen in the L_{max}-P_0 plane. In the low power region, L_{max} increases with increasing P_0 but at a lower slope compared with single-channel transmission. In the second region, corresponding to high launch power, L_{max} decreases with increasing P_0. Careful investigation indicates clearly that the origin of this behavior is the nonlinear fiber optics and mainly due to FWM process. When the nonlinear refractive index parameter n_2 in the used software is set to zero, the L_{max}-P_0 relation for both single-channel and WDM links become almost identical. Recall that n_2 = 0 means that the fiber refractive index becomes intensity independent and therefore, Kerr effect vanishes.

To get clear view about the effect of FWM, the spectra of the WDM waveforms at the multiplexer output and the fiber end are recorded for different operating conditions covering the following scenarios

Scenario A-4-4: 4-PAM 4-channel interconnect
Scenario A-8-4: 8-PAM 4-channel interconnect
Scenario A-4-8: 4-PAM 8-channel interconnect
Scenario A-8-8: 8-PAM 8-channel interconnect.

There are also four ideal Scenarios covering the above operating conditions but without the effect of nonlinear fiber optics (i.e., n_2=0) and denoted here by Scenarios B-4-4, B-8-4, B-4-8, and B-8-8, respectively.

Figure 7 shows the waveforms spectra associated with Scenario A-4-4 (i.e., 4-PAM 4-channel link) when the channel launch power P_0 equals 0 dBm and for three values of fiber length 20, 40, and 60 km. The simulation is repeated for P_0 =10 dBm and the results are displayed in Fig. 8. The results related to the Scenarios A-8-4, A-4-8, A-8-8 are depicted in Appendix [Figs. (20 and 21), (22 and 23), and (24 and 25), respectively]. Results related to group B Scenarios (i.e., n_2 = 0) are included in Figs. 9 and 10 for P_0 equals 0 and 10 dBm, respectively. Comparing the results in Figs. 7, 8, and 20 to 25 highs light the following facts

i. The level of the FWM component increases with launch power (which is an expected results) while the number of the generated FWM components are increasing function of both launch power and transmission distance which indicates the presence of cascaded FWM.
ii. The above observation is more pronounced when number of channels and PAM order increase. In fact, increasing number of multiplexed channels means increasing the total optical intensity in the fiber core which enhances the nonlinear phenomenon further according to Kerr effect.

The effect of nonlinear fiber optics of the received eye diagram is also investigated for the PAM WDM interconnect. The results are presented in Figs. 11-13 for the 4-PAM 8-channel link. Figures 11 to 13 show the eye diagrams after 20 km transmission for channels 1, 5, and 8 assuming 0, 5, and 10 dBm channel launch power, respectively. Channels 1 and 8 represent the edge channels in the WDM signal spectrum while channel 5 represents the central channel in this spectrum. The 20 km distance is chosen here because the received eye diagram corresponding to a single-channel transmission is completely opened even at 0 dBm launch power. The results in these figures reveal the following findings.

The central channel (Ch.5) is more affected by FWM compared with edge channels (Ch.1 and Ch.8). Recall that in DFWM process, two photons of the ith channel produce two FWM photons, one with higher frequency (f_i+Δf) and one with low frequency (f_i-Δf). Therefore, Ch.5 is affected by FWM components generated by both higher-index (higher-frequency) channels (mainly from Ch.6) and lower-index (lower-frequency) channels (mainly from Ch.4). In contrast, Ch.1 is affected by FWM components from

higher-index channels (mainly from Ch.2) while Ch.2 is affected by lower-index channels (mainly Ch.7).

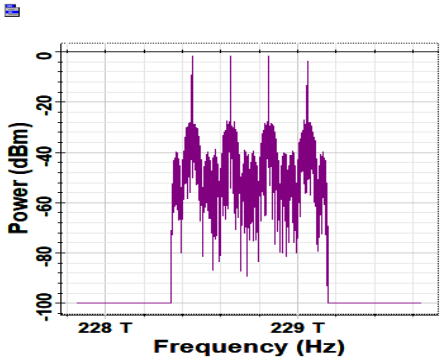

(a)

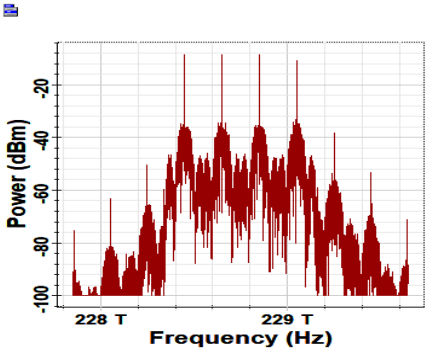

(b)

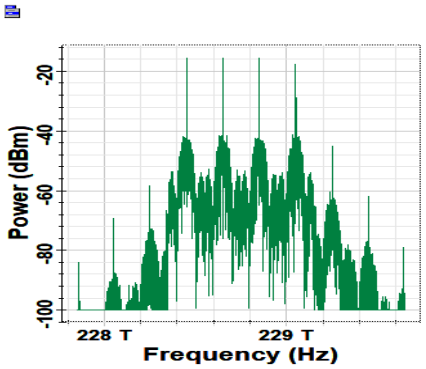

(c)

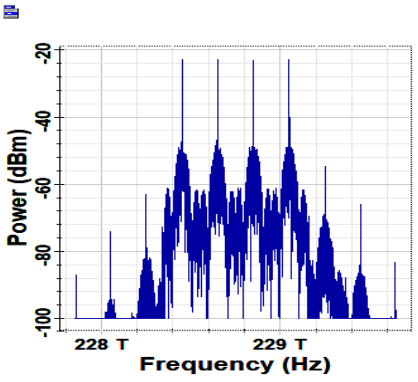

(d)

Figure 7. Spectra corresponding to 4-PAM 4-channel WDM link operating with 0 dBm channel launch power (a) multiplex output (b)-(d) optical spectrum at the end of 20, 40, and 60 km fiber, respectively

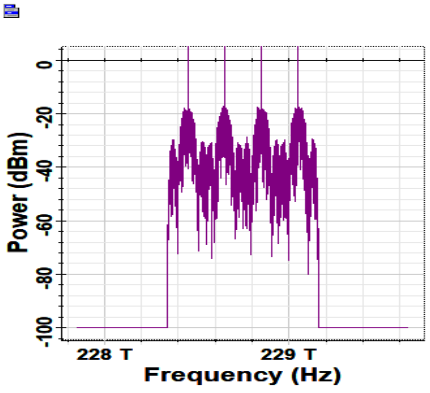

(a)

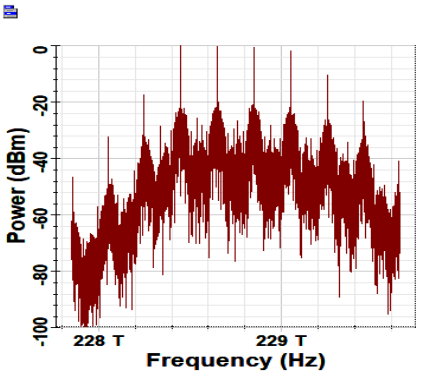

(b)

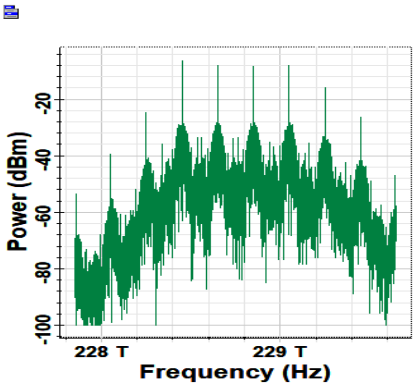

(c)

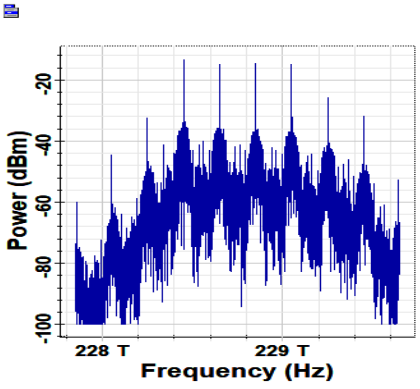

(d)

Figure 8. Spectra corresponding to 4-PAM 4-channel WDM link operating with 10 dBm channel launch power (a) multiplex output (b)-(d) optical spectrum at the end of 20, 40, and 60 km fiber, respectively

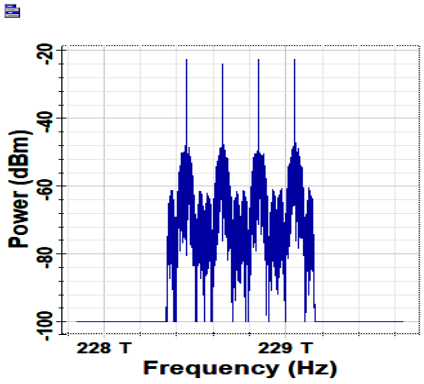

(a)

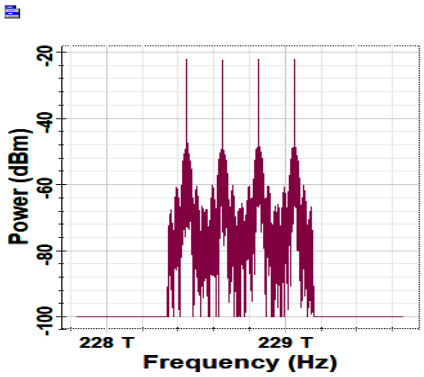

(b)

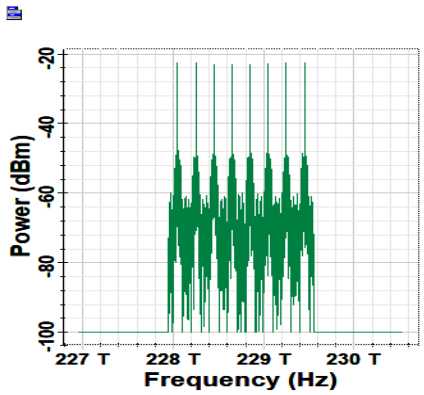

(c)

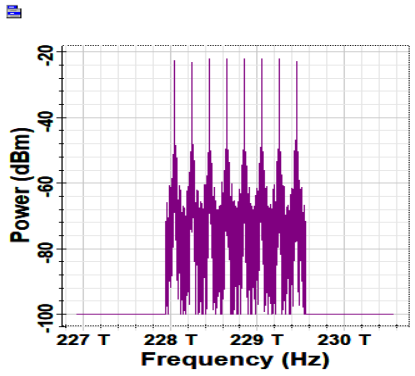

(d)

Figure 9. Received optical waveforms spectra corresponding to the four group B Scenarios. 60 km of fiber having $n_2 = 0$ is used with 0 dBm channel launch power (a) 4-PAM 4-channel (b) 8-PAM 4-channel (c) 4-PAM 8-channel (d) 8-PAM 8-channel

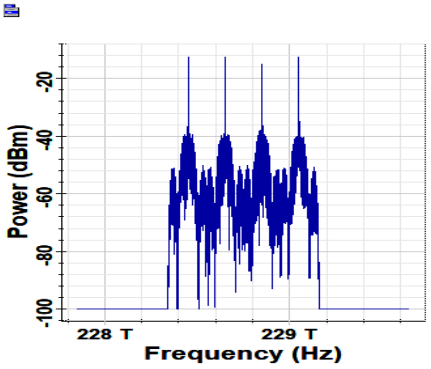

(a)

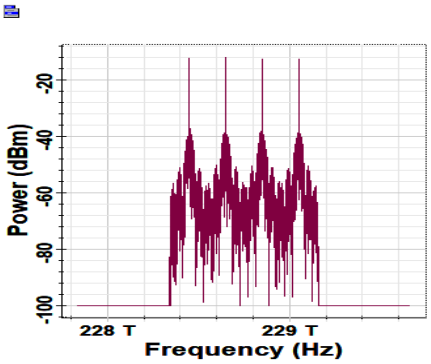

(b)

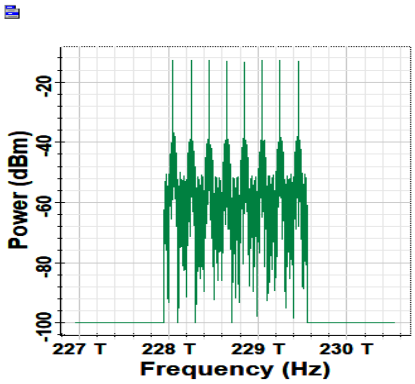

(c)

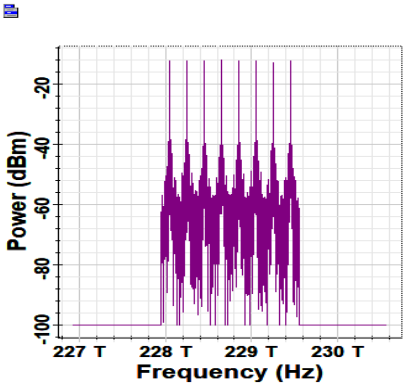

(d)

Figure 10. Received optical waveforms spectra corresponding to the four group B Scenarios. 60 km of fiber having $n_2 = 0$ is used with 10 dBm channel launch power (a) 4-PAM 4-channel (b) 8-PAM 4-channel (c) 4-PAM 8-channel (d) 8-PAM 8 -channel

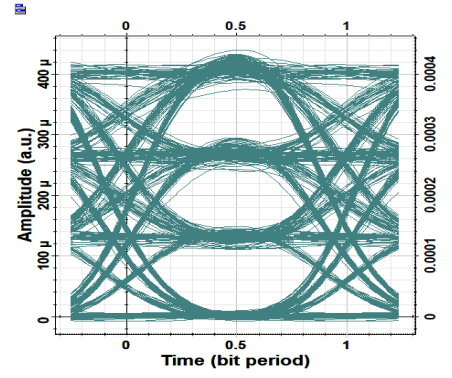

(a)

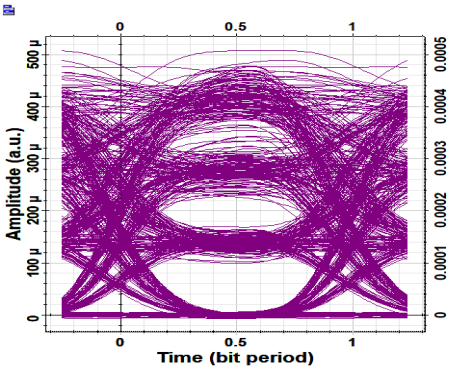

(b)

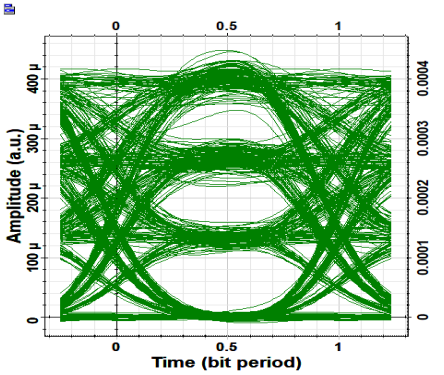

(c)

Figure 11. Received eye diagrams for 4-PAM 8-channel link at 0 dBm launch power and 20 km transmission (a) Ch.1 (b) Ch.5 (c) Ch.8

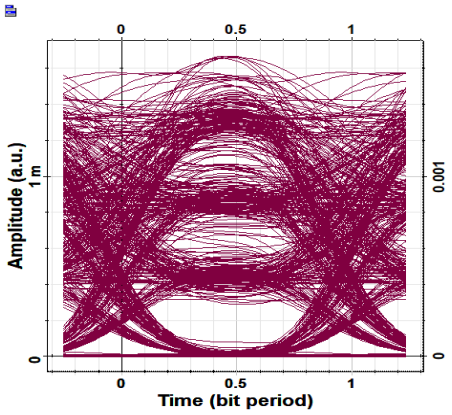

(a)

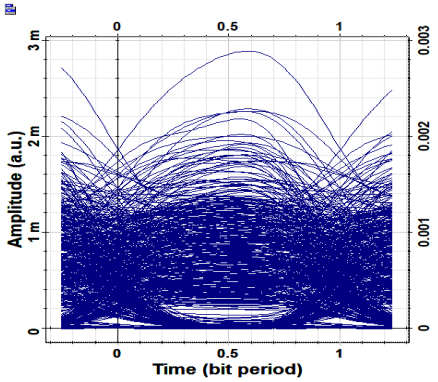

(b)

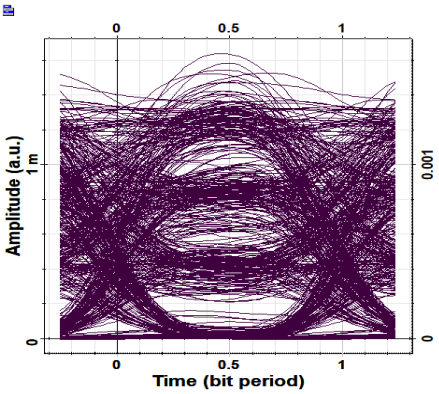

(c)

Figure 12. Received eye diagrams for 4-PAM 8-channel link at 5 dBm launch power and 20 km transmission (a) Ch.1 (b) Ch.5 (c) Ch.8

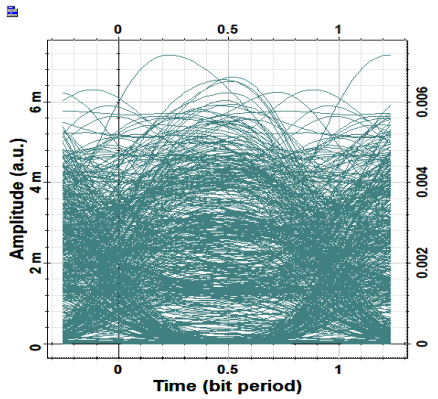

(a)

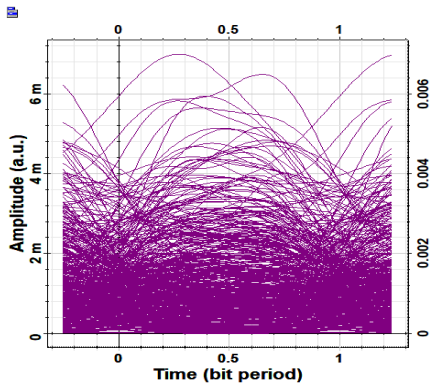

(b)

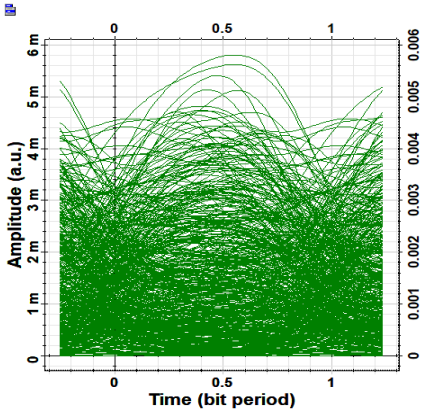

(c)

Figure 13. Received eye diagrams for 4-PAM 8-channel link at 10 dBm launch power and 20 km transmission (a) Ch.1 (b) Ch.5 (c) Ch.8

Increasing the channel launch power P_0 degrades the quality of the received eye diagram due to the increase in the associated nonlinear fiber optics level. Note that at P_0 = 0 dBm, the eye diagrams of the three channels under observation are almost opened. At P_0 = 5 dBm, the eye opening of Ch.1 and Ch.8 reduces, while the eye diagram of Ch.5 is almost closed. Increasing P_0 further to 10 dBm yields completely closed eye diagrams for the three channels.

It is worth to mention here the degradation in the quality of the received eye diagrams noticed above is due to nonlinear fiber optics and not due to fiber loss. The reasons behind this claim is that the received eye diagram corresponding to 20 km transmission is completely opened. To justify this claim further, the eye diagrams corresponding to the transmission of 8-chanel WDM signal over 60 km with 10 dBm launch power are recorded for channels 1, 5, and 8 after turning off the nonlinear refractive index parameters n_2, in the software package. The results are depicted in Figs. 14 and 15 for 4- and 8-PAM interconnects, respectively, and indicate clearly that the eye diagrams are opened even when high launch power (10 dBm) and long distance (60 km) are used in the simulation. These eye diagrams are almost similar to the eye diagram related to a single-channel transmission operating at the same WDM-channel conditions but with n_2 is turned ON in the software.

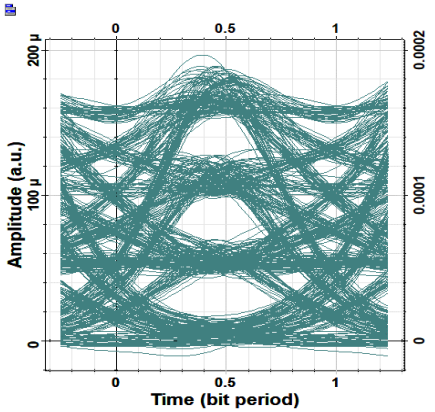

(a)

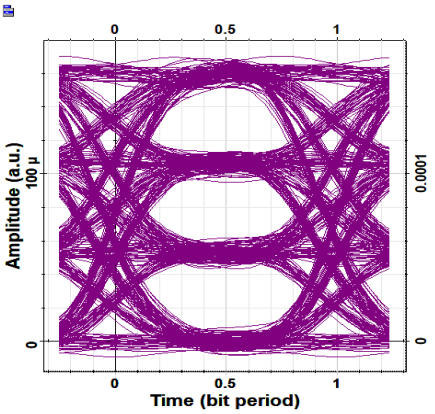

(b)

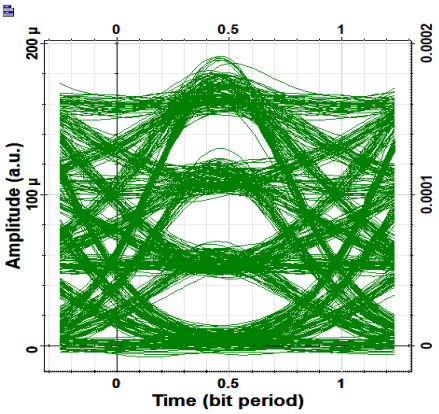

(c)

Figure 14. Eye diagrams corresponding to the transmission over 60 km of fiber having n_2 = 0 and with 10 dBm launch power for 4-PAM 8-WDM (a) Ch.1 (b) Ch.5 (c) Ch.8

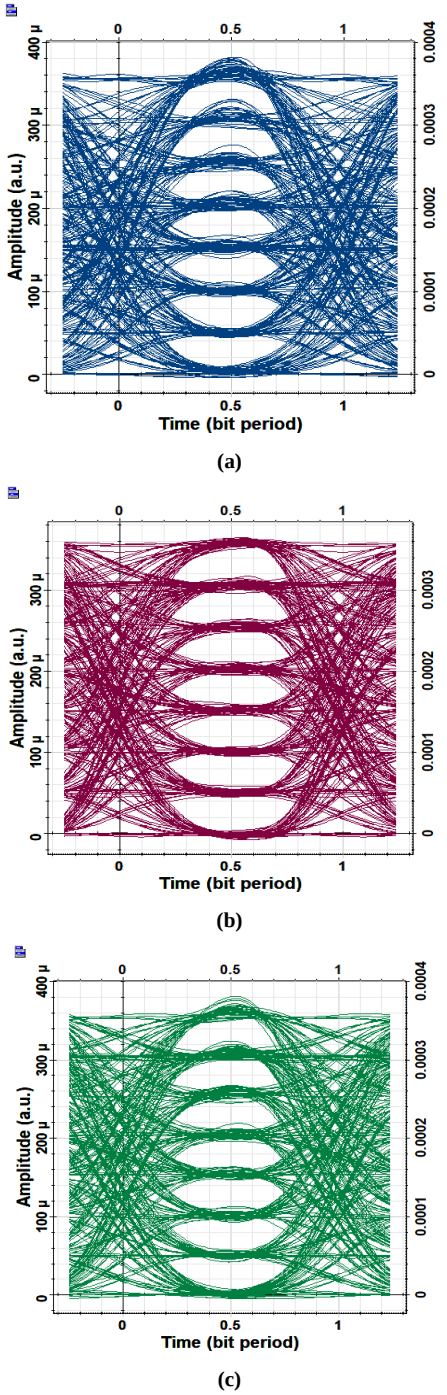

Figure 15. Eye diagrams corresponding to the transmission over 60 km of fiber having $n_2 = 0$ and with 10 dBm launch power for 8-PAM 8-WDM (a) Ch.1 (b) Ch.5 (c) Ch.8

4. Designing the PAM WDM Interconnect with Polarization Interleaving

It is well-know that most of the nonlinear mixing processes between two electromagnetic waves depend on the cross product of their polarization field vectors. Generally, the efficiency of the mixing process depends on $\cos(\Delta\theta_P)$, where $\Delta\theta_P$ is the phase difference between their polarization angles. Therefore, the effect of mixing vanishes when the two waves have orthogonal polarizations (i.e., $\Delta\theta_P=0$). These concepts have been already noticed in nonlinear fiber optics and the impact of interchannel nonlinear effects can be reduced considerably by ensuring that the neighboring channels are orthogonally polarized [38]. The same idea has been applied for high-bit rate long-haul optical communication systems to reduce interchannel nonlinearities [39, 40].

In this work, the concept of polarization interleaving is applied to reduce the effects of fiber nonlinear optics on the performance of the designed PAM WDM interconnects. Two polarization interleaved (PI) WDM configurations are introduced here as shown in Figs. 16a and 16b. In Fig. 16a, a polarization controller (PC) is inserted at the output of each transmitter laser to control its state of polarization (SOP) before entering the multiplexer. The SOPs of the odd and even lasers should be orthogonal at the outputs of the polarization controllers. For example, in the 8-channel WDM link, the polarizations of the fields of lasers 1, 3, 5 and 7 are aligned in the x direction while the field polarizations of the lasers 2, 4, 6 and 8 are aligned in the y direction. This configuration is called here PI-WDM1 interconnect.

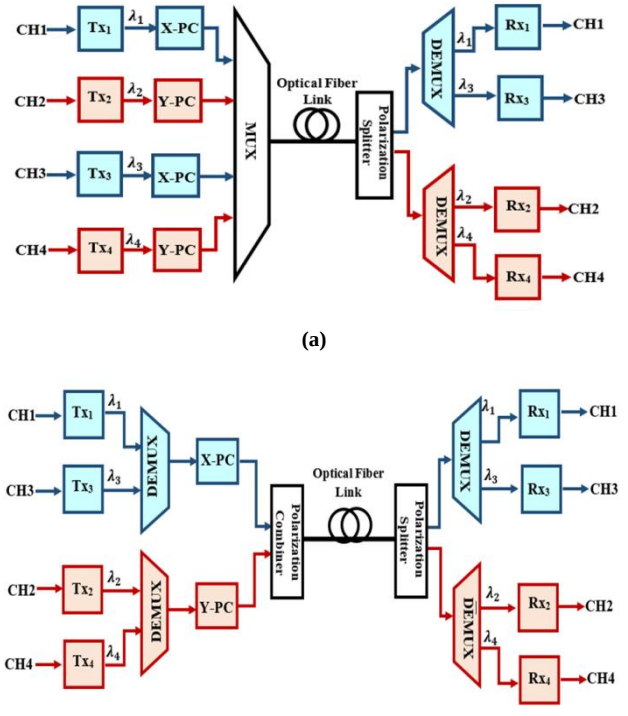

Figure 16. Configurations of WDM interconnect with polarization controller (a) PI-WDM1 interconnect (b) PI-WDM2 interconnect. Tx: PAM optical transmitter, Rx: PAM optical receiver, X-PC and Y-PC: polarization controllers, X and Y denote X- and Y-Polarizations, respectively

In the configuration of Fig. 16b, which is denoted here by PI-WDM2 interconnect, two separate multiplexers are used.

One of the multiplexer is used to groups the odd number channels while the other multiplexer groups the even number channels. Two wideband PCs are used, each one is inserted at the output of each multiplexer, to ensure that the SOPs of the two WDM waveforms are orthogonal.

Simulation tests are performed to address the performance of the two PI-interconnects. The results reveal that both interconnects have almost identical performance if the used PCs are designed to control sharply the required SOP over the operating wavelength range. The IP-WDM1 interconnect uses N narrowband PCs. (In this work, 200 GHz PCs are used). The IP-WDM2 interconnect uses two wideband PCs. (In this work, two 1.6 THz PCs are employed for the 8-channel interconnects). Such wideband PC is costly and needs careful design considerations.

To get clear picture about the key role played by the polarization interleaving, the four WDM interconnects described by group A Scenarios are simulated in the presence polarization interleaving assuming 20 km SSMF link. The results are presented in Figs. 17 and 18 for 0 and 5 dBm launch power per channel, respectively. Each figure contains the optical spectrum of the received waveform and the corresponding central channel eye diagram for each of the four interconnects.

It is clear from these figures that the polarization interleaving works well in the 4-channel WDM link even with 8-PAM and 5 dBm launch power leading to almost perfect eye diagram at the receiver side. In contrast, the improvement in the quality of the received eye diagram gained by using polarization interleaving in the 8-channel WDM link is reduced compared to the 4-channel WDM link. The reduction in the quality of the eye diagram is more pronounced for the 8-PAM when the launch power increases. At P_0 =5 dBm, the eye diagram corresponding to 20 km transmission over 8-PAM 8-WDM link is almost closed.

5. Summary of the Transmission Performance of the Designed O-Band PAM WDM Interconnects

The simulation is carried further to deduce the variation of maximum transmission distance L_{max} with channel launch power P_0 for the designed WDM interconnects operating with and without polarization interleaving. The results are presented in Figs. 19a-d for the four interconnect described in group A Scenarios (namely, 4-PAM 4-WDM, 4-PAM 8-WDM, 8-PAM 4-WDM, and 8-PAM 8-WDM). Additional results corresponding to the ideal case when the effect of fiber nonlinear optics in neglected (i.e., $n_2 = 0$) are also included in these figures for comparison purposes. Note that the transmission performance corresponding to $n_2 = 0$ cases is independent of number of multiplexed channels and the results match that of a single-channel counterpart.

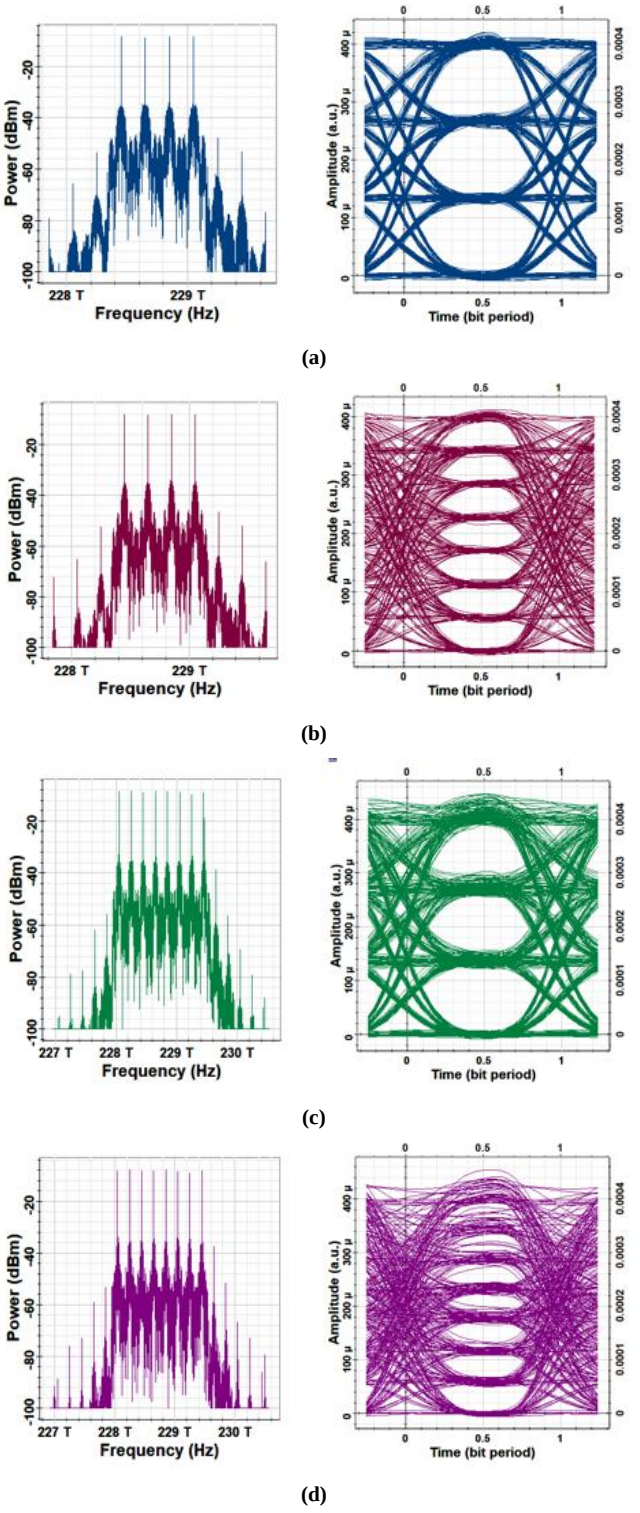

Figure 17. Optical spectrum and central channel eye diagram for different interconnects simulated with 0 dBm channel launch power and 20 km transmission distance and using polarization interleaving (a) 4-PAM 8-WDM (b) 8-PAM 4-WDM (c) 4-PAM 8-WDM (d) 8-PAM 8-WDM. The central channels under observation are the third and fifth in 4- and 8-channel WDM link, respectively

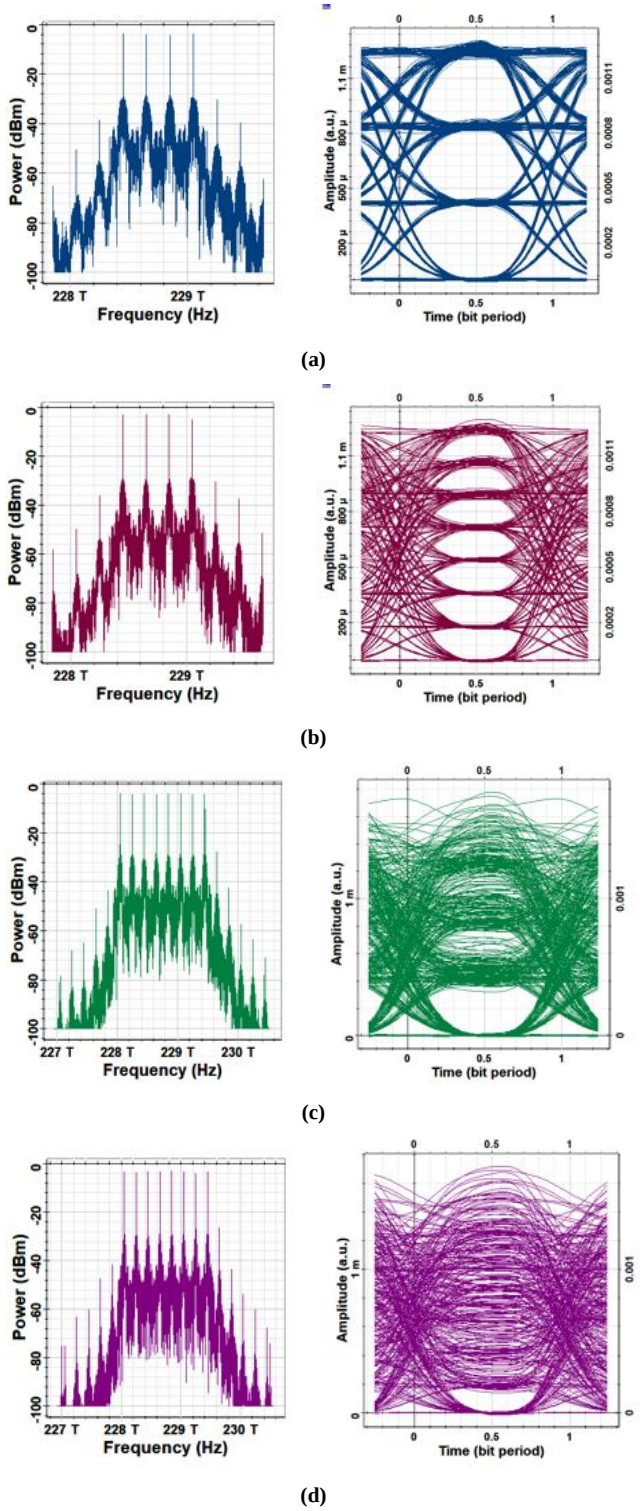

Figure 18. Optical spectrum and central channel eye diagram for different interconnects simulated with 5 dBm channel launch power and 20 km transmission distance and using polarization interleaving (a) 4-PAM 8-WDM (b) 8-PAM 4-WDM (c) 4-PAM 8-WDM (d) 8-PAM 8-WDM. The central channels under observation are the third and fifth in 4- and 8-channel WDM link, respectively

The following conclusions are drawn from the results depicted in Figs. 19a-d

i. In the presence of polarization interleaving, the maximum reach L_{max} approaches its highest value, L_{opt}, at a certain level of launch power (called here optimum launch power P_{opt}). The optimum values P_{opt} and L_{opt} depend on the PAM order and number of multiplexed channels (see Table 1). For each of the four interconnects, the transmission distance increases with P_0 when $P_0<P_{opt}$. Operating with $P_0 > P_{opt}$ leads to decrease L_{max} with increase of P_0 due to nonlinear effects. The highest values of P_{opt} and L_{opt} occurs in the 4-PAM 4-WDM interconnect (7 dBm and 62 km). These values reduce with increasing PAM order and/or number of multiplexed channels.

ii. Operating with polarization interleaving and with $P_0 < P_{opt}$ shows that the variation of the transmission distance L_{max} with P_0 almost matches the relation of the single-channel transmission (i.e., $n_2 = 0$ case). This statement is true except for the 8-PAM 8-channel WDM link where the value of L_{max} is less than that of the single-channel transmission. This is due to the high level of nonlinear fiber optics in this case.

iii. The presence of polarization interleaving enhances the maximum reach compared with similar link designed without PI as shown in Table 2.

Table 1. Optimum performance parameters for the polarization interleaved WDM interconnects

Interconnect Type	Optimum Channel power P_{opt} (dBm)	Optimum Transmission Distance L_{opt} (km)	Bit Rate-Distance Product (Tbps.km)
4-PAM 4-WDM	7	62	27.8
8-PAM 4-WDM	6	48	21.5
4-PAM 8-WDM	3	47	42.1
8-PAM 8-WDM	3	14	12.5

Table 2. Maximum transmission in the absence and presence of polarization interleaving (a) 4-channel WDM interconnect (b) 8-channel WDM interconnect. "X" denotes that the transmission distance is less than 1 km

(a) 4-channel WDM interconnect

Launch Power (dBm)	Maximum Transmission (km)			
	4-PAM		8-PAM	
	Without PI	With PI	Without PI	With PI
0	38	44	8	36
1	40	47	5	39
2	30	50	3	42
3	8	54	X	44
4	1	56	X	46

(b) 8-channel WDM interconnect

Launch Power (dBm)	Maximum Transmission (km)			
	4-PAM		8-PAM	
	Without PI	With PI	Without PI	With PI
0	10	42	2	10
1	5	45	1	12
2	3	46	1	13
3	1	47	X	14
4	X	20	X	4

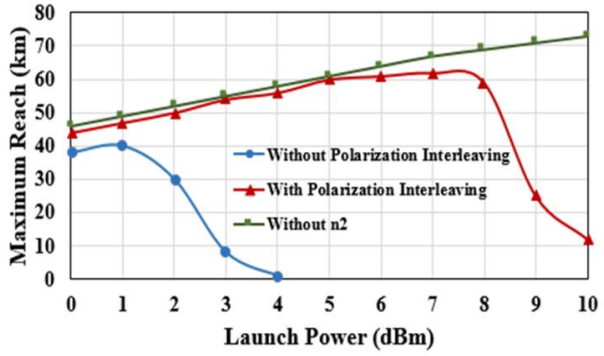

(a)

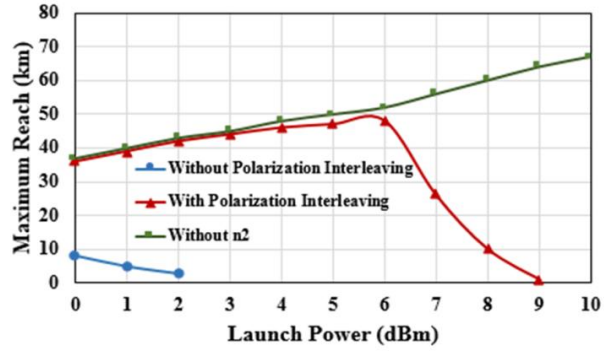

(b)

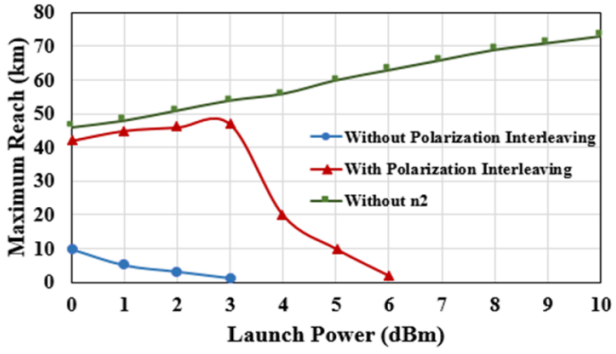

(c)

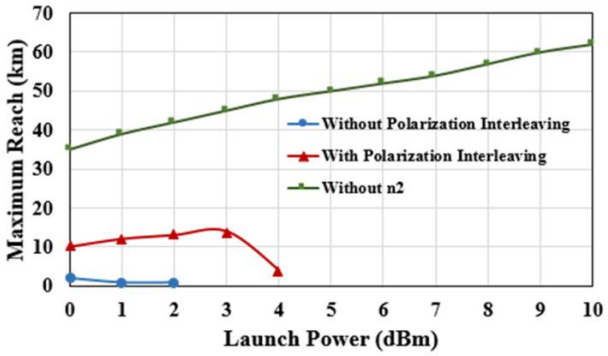

(d)

Figure 19. Variation of maximum transmission with channel launch power for four different WDM interconnects (a) 4-PAM 4-WDM (b) 8-PAM 4-WDM (c) 4-PAM 8-WDM (d) 8-PAM 8-WDM

6. Conclusions

The transmission performance of unamplified 4×112 Gbps and 8×112 Gbps WDM-based data center interconnects has been investigated for O-band operation using 200 GHz channel spacing. The single WDM channel uses IM/DD scheme with 4- and 8-PAM modulation formats. The analytical and simulation results reveal that the effect of FWM on the performance of O-band WDM interconnect is more severe compared with C-band counterpart. The effect of FWM is more pronounced with 8-PAM 8-channel WDM interconnects compared with other PAM-WDM links. Polarization interleaving (PI) technique has been used to reduce the effect of FWM on the transmission performance of the WDM interconnects using PI with 0 dBm channel launch power increases the maximum reach L_{max} to 44, 36, 42, and 10 km for 4-PAM 4-WDM, 8-PAM 4-WDM, 4-PAM 8-WDM, and 8-PAM 8-WDM interconnects, respectively. These values ate to be compared with 54, 44, 47, and 14 km, respectively, at 3 dBm launch power. The analysis and simulation results can be used as a guideline to design PAM–based O-band WDM interconnects. The work may be extended in the future to address the performance of 224 Gbps per channel PAM-WDM interconnects and to introduce 16-PAM modulation in the investigation.

Appendix

Results related to the Scenarios A-8-4, A-4-8, A-8-8 for M-PAM WDM interconnects.

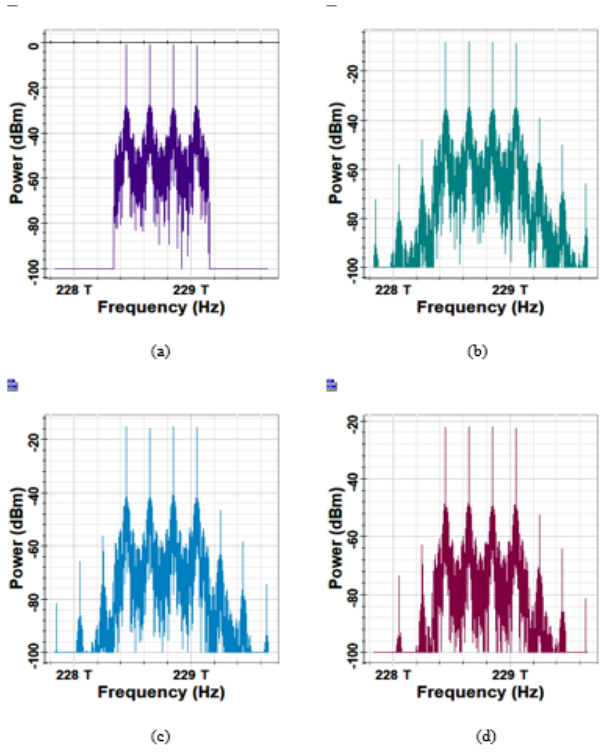

Figure 20. Spectra corresponding to 8-PAM 4-channel WDM link operating with 0 dBm channel launch power (a) multiplex output (b)-(d) optical spectrum at the end of 20, 40, and 60 km fiber, respectively

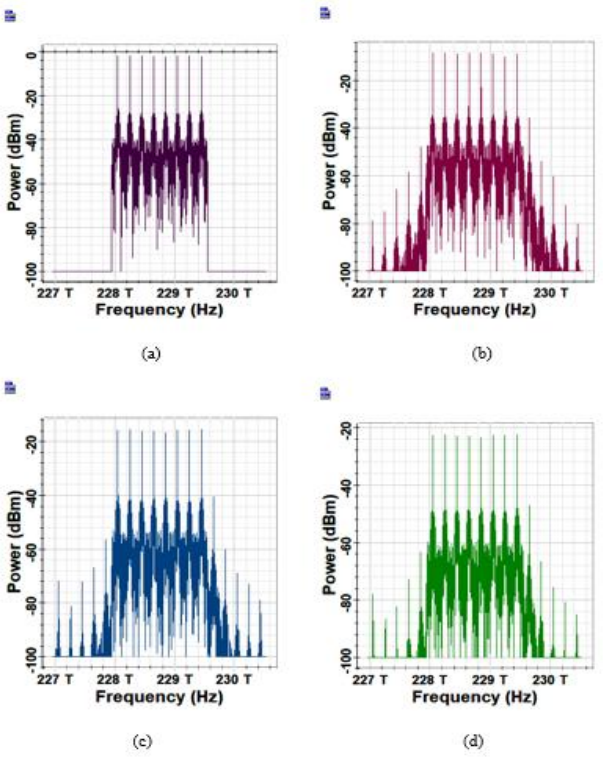

Figure 22. Spectra corresponding to 4-PAM 8-channel WDM link operating with 0 dBm channel launch power (a) multiplex output (b)-(d) optical spectrum at the end of 20, 40, and 60 km fiber, respectively

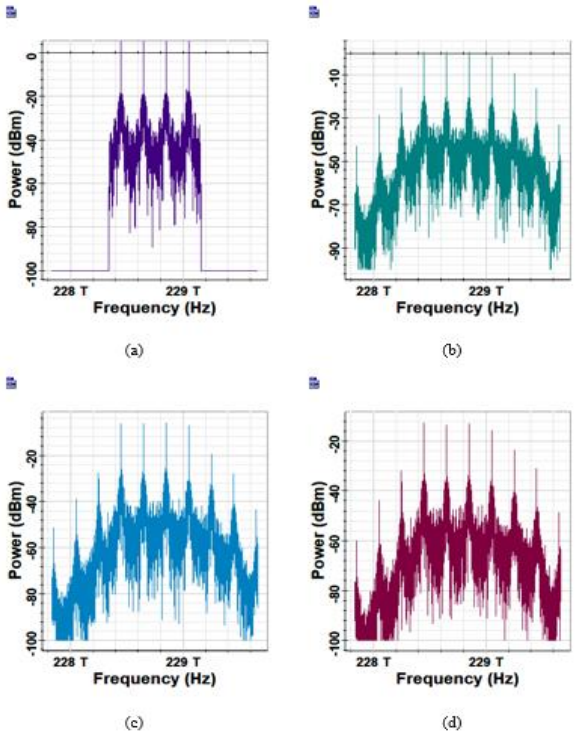

Figure 21. Spectra corresponding to 8-PAM 4-channel WDM link operating with 10 dBm channel launch power (a) multiplex output (b)-(d) optical spectrum at the end of 20, 40, and 60 km fiber, respectively

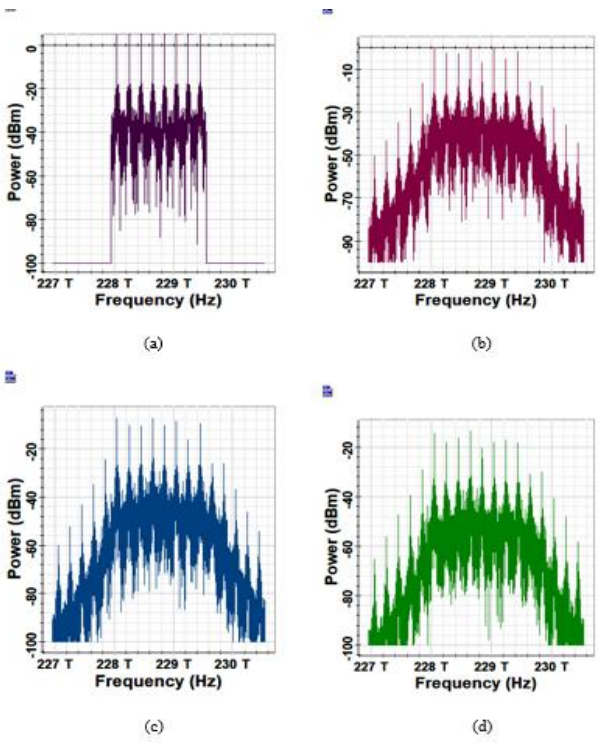

Figure 23. Spectra corresponding to 4-PAM 8-channel WDM link operating with 10 dBm channel launch power (a) multiplex output (b)-(d) optical spectrum at the end of 20, 40, and 60 km fiber, respectively

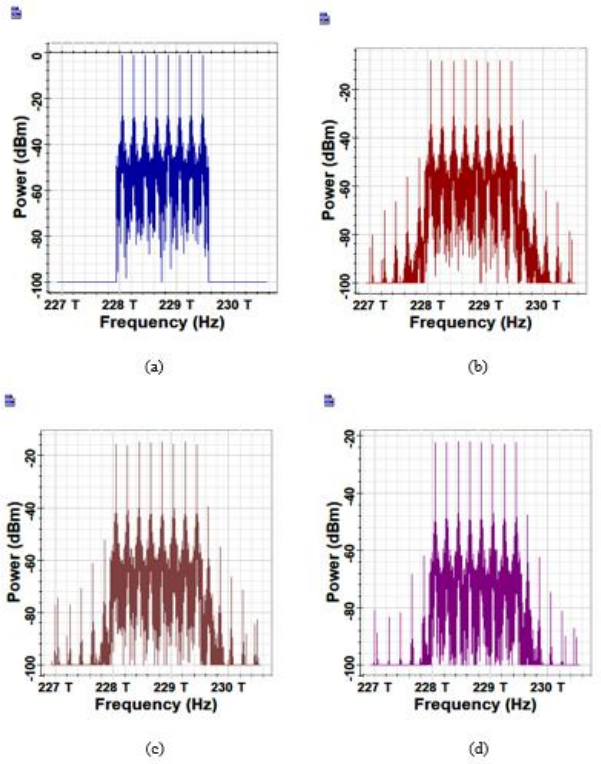

Figure 24. Spectra corresponding to 8-PAM 8-channel WDM link operating with 0 dBm channel launch power (a) multiplex output (b)-(d) optical spectrum at the end of 20, 40, and 60 km fiber, respectively

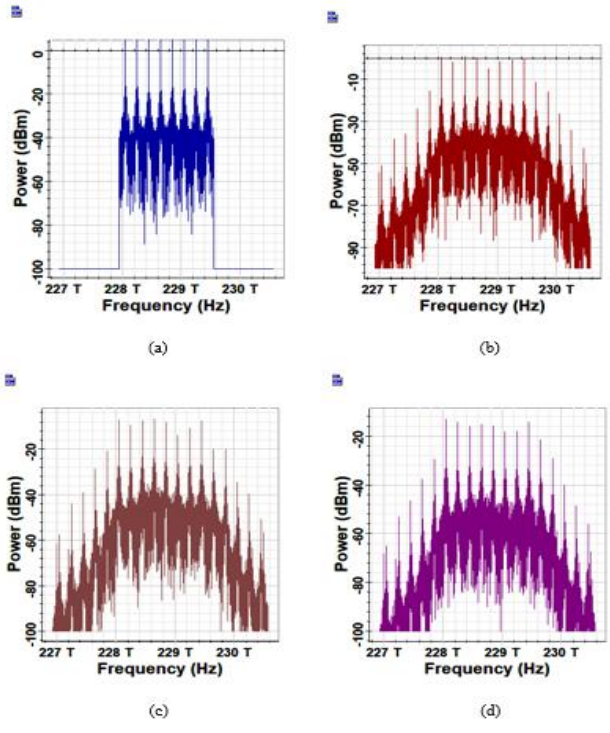

Figure 25. Spectra corresponding to 8-PAM 8-channel WDM link operating with 10 dBm channel launch power (a) multiplex output (b)-(d) optical spectrum at the end of 20, 40, and 60 km fiber, respectively

REFERENCES

[1] J. Cai, H. G. Batshon, M. V. Mazurczyk, O. V. Sinkin, D. Wang, M. Paskov, W. W. Patterson, C. R. Davidson, P. C. Corbett, G. M. Wolter, T. E. Hammon, M. A. Bolshtyansky, D. G. Foursa and A. N. Pilipetskii, "70.46 Tb/s over 7,600 km and 71.65 Tb/s over 6,970 km transmission in C+L band using coded modulation with hybrid constellation shaping and non-linearity compensation," IEEE Journal of Lightwave Technology, vol. 36, no. 1, pp. 114-121, Jan. 2018.

[2] N. Suzuki, H. Miura, K. Matsuda, R. Matsumoto, and K. Motoshima, "100 Gb/s to 1 Tb/s based coherent passive optical network technology," IEEE Journal of Lightwave Technology, vol. 36, no. 8, pp. 1485-1491, Apr. 2018.

[3] K. Kimura, J. Nitta, M. Yoshida, K. Kasai, T. Hirooka, and M. Nakazawa, "Single-channel 7.68 Tbit/s, 64 QAM coherent Nyquist pulse transmission over 150 km with a spectral efficiency of 9.7 bit/s/Hz," Optics Express, vol. 26, no. 13, pp. 17418- 17428, Jun. 2018.

[4] D. Soma, Y. Wakayama, S. Beppu, S. Sumita, T. Tsuritani, T. Hayashi, T. Nagashima, M. Suzuki, M. Yoshida, K. Kasai, M. Nakazawa, H. Takahashi, K. Igarashi, I. Morita, and M. Suzuki, "10.16-Peta-B/s dense SDM/WDM transmission over 6-Mode 19-core fiber across the C+L band," IEEE Journal of Lightwave Technology, vol. 36, no. 6, pp. 1362-1368, Mar. 2018.

[5] Y. Hsu, C. Y. Chuang, X. Wu, G. H. Chen, C. W. Hsu, Y. C. Chang, C. W. Chow, J. Chen, Y. C. Lai, C. H. Yeh, and H. K. Tsang, "2.6 Tbit/s on-chip optical interconnect supporting mode-division-multiplexing and PAM-4 signal," IEEE Photonics Technology Letters, vol. 30, no. 11, pp. 1052-1055, Jun. 2018.

[6] N. Eiselt, J. Wei, H. Griesser, A. Dochhan, M. H. Eiselt, J. P. Elbers, J. J. V. Olmos, and I. T. Monroy, "Evaluation of real-time 8x56.25 Gb/s (400G) PAM-4 for inter-data center ap-plication over 80 km of SSMF at 1550 nm," IEEE Journal of Lightwave Technology, vol. 35, no. 4, pp. 955-962, Feb. 2017.

[7] C. Prodaniuc, N. Stojanovic, F. Karinou, Z. Qiang, and R. Llorente, "Performance comparison between 4D trellis coded modulation and PAM-4 for low-cost 400 Gbps WDM optical networks," IEEE Journal of Lightwave Technology, vol. 34, no. 22, pp. 5308-5316, Nov. 2016.

[8] S. Ohlendorf, S. Pachnicke, and W. Rosenkranz, "Multidimensional PAM with pseudo-gray coding for flexible data center interconnects," IEEE Photonics Technology Letters, vol. 30, no. 12, pp. 1143-1146, Jun. 2018.

[9] R. Rao, T. Fukui, R. Hirai, N. Kikuchi, "400GbE using Nyquist PAM4 for 2km and 10km PMD," Oclaro, pp. 1-11, Sept. 2014.

[10] G. Khanna, T. Rahman, E. D. Man, E. Riccardi, A. Pagano, A. C. Piat, S. Calabrò, B. Spinnler, D. Rafique, U. Feiste, H. D. Waardt, B. S. Krombholz, N. Hanik, T. Drenski, M. Bohn, and A. Napoli, "Single-carrier 400G 64QAM and 128QAM DWDM field trial transmission over metro legacy links," IEEE Photonics Technology Letters, vol. 29, no. 2, pp. 189-192, Jan. 2017.

[11] M. M. Osman, M. Chagnon, M. Poulin, S. Lessard, and D. V. Plant, "224-Gb/s 10-km transmission of PDM PAM-4 at 1.3

μm using a single intensity-modulated laser and a di-rect-detection MIMO DSP-based receiver," IEEE Journal of Lightwave Technology, vol. 33, no. 7, pp. 1417-1424, Apr. 2015.

[12] H. Mardoyan, M. A. Mestre, J. M. Estar´an, F. Jorge, F. Blache, P. Angelini, A. Konczykowska, M. Riet, V. Nodji-adjim, J. Dupuy, and S. Bigo, "84-, 100-, and 107-GBd PAM-4 intensity modulation direct-detection transceiver for datacenter interconnects", IEEE Journal of Lightwave Tech-nology, vol. 35, no. 6, pp. 1253-1259, Mar. 2017.

[13] P. Dong, A. Maho, R. Brenot, Y. K. Chen, and A. Melikyan, "Directly reflectivity modulated laser," IEEE Journal of Lightwave Technology, vol. 36, no. 5, pp. 1255-1261, Mar. 2018.

[14] E. E. Fiky, M. Osman, M. Sowailem, A. Samani, D. Patel, R. Li, M. G. Saber, Y. Wang, N. Abadia, Y. D'mello, and D. V. Plant, "200 Gb/s transmission using a dual-polarization O-Band silicon photonic intensity modulator for Stokes vector direct detection applications," Optics Express, vol. 25, no. 24, pp. 30336 - 30348, Nov. 2017.

[15] F. Karinou, C. Prodaniuc, N. Stojanovic, M. Ortsiefer, A. Daly, R. Hohenleitner, B. Kögel, and C. Neumeyr "Directly PAM-4 modulated 1530-nm VCSEL enabling 56 gb/s/ λ data-center interconnects", IEEE Photonics Technology Letters, vol. 27, no. 17, pp. 1872-1875, Sept. 2015.

[16] J. C. Cartledge and A. S. Karar, "100 Gb/s intensity modulation and direct detection," IEEE Journal of Lightwave Technology, vol. 32, no. 16, pp. 2809-2814, Aug. 2014.

[17] F. Gao, S. Zhou, X. Li, S. Fu, L. Deng, M. Tang, D. Liu, and Q. Yang, "2 × 64 Gb/s PAM-4 transmission over 70 km SSMF using O-band 18G-class directly modulated lasers (DMLs)," Optics Express, vol. 25, no. 7, pp. 7230-7237, Apr. 2017.

[18] Y. Wan, D. Inoue, D. Jung, J. C. Norman, C. Shang, A. C. Gossard, and J. E. Bowers, "Directly modulated quantum dot lasers on silicon with a milliampere threshold and high temperature stability," Photonics Research, vol. 6, no. 8, pp. 776-781, Aug. 2018.

[19] J. P. V. Engelen, L. Shen, G. Roelkens, Y. Jiao, M. K. Smit, and J. J. G. M. V. D. Tol, "A novel broadband elec-tro-absorption modulator based on bandfilling in n-InGaAs: design and simulations," IEEE Journal of Selected Topics in Quantum Electronics, vol. 24, no. 1, Article no. 3300108, Jan/Feb. 2018.

[20] Y. Zhu, K. Zou, Z. Chen, and F. Zhang, "224 Gb/s optical carrier-assisted Nyquist 16-QAM half-cycle single-sideband direct detection transmission over 160 km SSMF," IEEE Journal of Lightwave Technology, vol. 35, no. 9, pp. 1557-1565, May 2017.

[21] Z. Li, M. S. Erkılınc, K. Shi, E. Sillekens, L. Galdino, T. Xu, B. C. Thomsen, P. Bayvel, and R. I. Killey, "Digital linearization of direct-detection transceivers for spectrally efficient 100 Gb/s/λ WDM metro networking," IEEE Journal of Lightwave Technology, vol. 36, no. 1, pp. 27-36, Jan. 2018.

[22] K. Zou, Y. Zhu, and F. Zhang, "800 Gb/s (8×100 Gb/s) Nyquist half-cycle single-sideband modulation direct-detection transmission over 320 km SSMF at C-band," IEEE Journal of Lightwave Technology, vol. 35, no. 10, pp. 1900-1905, May 2017.

[23] E. El-Fiky, M. Chagnon, M. Sowailem, A. Samani, M. M. Osman, and D. V. Plant, "168-Gb/s single carrier PAM4 transmission for intra-data center optical interconnects," IEEE Photonics Technology Letters, vol. 29, no. 3, pp. 314-317, Feb. 2017.

[24] M. R.T. Tan, P. Rosenberg, W. V. Sorin, B. Wang, S. Mathai, G. Panotopoulos, and G. Rankin, "Universal photonic interconnect for data centers," IEEE Journal of Lightwave Technology, vol. 36, no. 2, pp. 175-180, Aug. 2017.

[25] X. Miao, M. Bi, Y. Fu, L. Li, and W. Hu, "Experimental study of NRZ, duobinary, and PAM-4 in O-band DML-based 100G-EPON," IEEE Photonics Technology Letters, vol. 29, no. 17, pp. 1490-1493, Sept. 2017.

[26] H. Y. Chen, N. Kaneda, J. Lee, J. Chen, and Y. K. Chen, "Optical filter requirements in an EML-based single-sideband PAM4 intensity-modulation and direct-detection transmission system," Optics Express, vol. 25, no. 6, pp. 5852- 5860, May 2017.

[27] X. Pang, O. Ozolins, S. Gaiarin, A. Kakkar, J. R. Navarro, M. I. Olmedo, R. Schatz, A. Udalcovs, U. Westergren, D. Zibar, S. Popov, and G. Jacobsen, "Experimental study of 1.55-μm EML-based optical IM/DD PAM-4/8 short reach systems," IEEE Photonics Technology Letters, vol. 29, no. 6, pp. 523-526, Mar. 2017.

[28] F. Li, X. Li, L. Chen, Y. Xia, C. Ge, and Y. Chen, "High-level QAM OFDM system using DML for low-cost short reach optical communications," IEEE Photonics Technology Letters, vol. 26, no. 9, pp. 941-944, May 2014.

[29] M. M. Osman, F. Fresi, E. Forestieri, M. Secondini, L. Potì, F. Cavaliere, S. Lessard, and D. V. Plant, "50 Gb/s short-reach interconnects with DSPfree direct-detection enabled by CAPS codes," Optics Express, vol. 26, no. 14, pp. 17916 - 17926, Jul. 2018.

[30] J. Tang, J. He, D. Li, M. Chen, and L. Chen, "64/128-QAM half-cycle subcarrier modulation for short-reach optical communications," IEEE Photonics Technology Letters, vol. 27, no. 3, pp. 284-287, Feb. 2015.

[31] H. Mardoyan, M. A. Mestre, R. Rios-M¨uller, A. Konczy-kowska, J. Renaudier, F. Jorge, B. Duval, J. Y. Dupuy, A. Ghazisaeidi, Ph. Jennev´e, M. Achouche, and S. Bigo, "Single carrier 168-Gb/s line-rate PAM direct detection transmission using high-speed selector power DAC for optical intercon-nects", IEEEE Journal of Lightwave Technology, vol. 34, no. 7, pp. 1593-1598, Apr. 2016.

[32] N. Stojanovic, F. Karinou, Z. Qiang, and C. Prodaniuc, "Volterra and wiener equalizers for short-reach 100G PAM-4 applications," IEEEE Journal of Lightwave Technology, vol. 35, no. 21, pp. 4583-4594, Nov. 2017.

[33] G. P. Agrawal, "Nonlinear Fiber Optics," 5th Edition, Academic Press, New York, USA, 2013.

[34] G. P. Agrawal, "Lightwave technology: Telecommunication systems," John Wiley, New York, USA, 2005.

[35] T. M. Bazan, "Impact of FWM on the performance of 2-D time-wavelength OCDMA systems," IEEE Journal of Lightwave Technology, vol. 35, no. 14, pp. 2846-2852, Jul. 2017.

[36] C. J. McKinstrie and M. Karlsson, "Effects of polarization-mode dispersion on degenerate four-wave mixing," IEEE Journal of Lightwave Technology, vol. 35, no. 19, pp. 4210-4218, Oct. 2017.

[37] J. Zyskind and A. Srivastava, "Optically amplified WDM networks," 1st Edition, Elsevier Science, USA, 2011.

[38] J. X. Cai, H. G. Batshon, M. V. Mazurczyk, O. V. Sinkin, D. Wang, M. Paskov, C. R. Davidson, W. W. Patterson, A. Turukhin, M. A. Bolshtyansky, and D. G. Foursa, "51.5 Tb/s capacity over 17,107 km in C+L bandwidth using single-mode fibers and nonlinearity compensation," IEEE Journal of Lightwave Technology, vol. 36, no. 11, pp. 2135-2141, Jun. 2018.

[39] H. J. Abd, N. M. Dinl, M. H. AI-Mansoori, F. Abdullahl and H. A. Fadhie, "Mitigation of FWM crosstalk in WDM system using polarization interleaving technique," IEEE 4th International Conference on Photonics, pp. 117-119, Dec. 2013.

[40] T. M. F. Alves and A. V. T. Cartaxo, "Analytical characterization of four wave mixing effect in direct-detection double-sideband OFDM optical transmission systems," Optics Express, vol. 22, no. 7, pp. 8598-8616, Apr. 2014.